Unusual regioversatility of acetyltransferase Eis, a cause of drug resistance in XDR-TB

Wenjing Chen[a,b,1], Tapan Biswas[c,1], Vanessa R. Porter[a,c], Oleg V. Tsodikov[b,c,2], and Sylvie Garneau-Tsodikova[a,b,c,2]

[a]Life Sciences Institute; [b]Chemical Biology Doctoral Program; and [c]Department of Medicinal Chemistry, University of Michigan, Ann Arbor, MI 48109

Edited* by Christopher T. Walsh, Harvard Medical School, Boston, MA, and approved April 30, 2011 (received for review April 4, 2011)

The emergence of multidrug-resistant and extensively drug-resistant (XDR) tuberculosis (TB) is a serious global threat. Aminoglycoside antibiotics are used as a last resort to treat XDR-TB. Resistance to the aminoglycoside kanamycin is a hallmark of XDR-TB. Here, we reveal the function and structure of the mycobacterial protein Eis responsible for resistance to kanamycin in a significant fraction of kanamycin-resistant *Mycobacterium tuberculosis* clinical isolates. We demonstrate that Eis has an unprecedented ability to acetylate multiple amines of many aminoglycosides. Structural and mutagenesis studies of Eis indicate that its acetylation mechanism is enabled by a complex tripartite fold that includes two general control non-derepressible 5 (GCN5)-related *N*-acetyltransferase regions. An intricate negatively charged substrate-binding pocket of Eis is a potential target of new antitubercular drugs expected to overcome aminoglycoside resistance.

bacterial resistance | product-bound complex | ribosome inhibitor | catalytic efficiency | crystal structure

Tuberculosis (TB) is a deadly infectious disease caused by the bacterium *Mycobacterium tuberculosis* (*Mtb*). With over 9 million new cases and nearly 2 million deaths each year, TB is one of the most serious health problems worldwide. Continuous use of the same multidrug therapy needed to treat TB and noncompliance have led to emergence of multidrug-resistant and extensively drug-resistant (XDR) strains of *Mtb*, an alarming problem due to their global spread. *Mtb* strains are classified as XDR when they are resistant to the two most potent first-line oral antituberculosis drugs, rifampicin and isoniazid, as well as to a fluoroquinolone and to at least one of three second line-injectable antituberculosis drugs [kanamycin A (KAN), amikacin (AMK), and capreomycin] (1).

KAN and AMK belong to the aminoglycoside (AG) family of antibiotics (2) that inhibit protein synthesis in bacteria by targeting the 16S rRNA of the 30S subunit (3, 4) of the ribosome (5). Recently, mechanisms of clinical resistance of *Mtb* to KAN were elucidated. In one-third of clinical isolates, encompassing a large set of strains from different regions of the world, clinical resistance to KAN was solely due to the upregulation of the chromosomal *eis* (enhanced intracellular survival) gene bearing mutations in its promoter (6). In the other two-thirds, the resistance was due to ribosomal mutations. A previous study established that increased expression of the AG acetyltransferase (AAC) Eis, encoded by the *eis* gene harboring such mutations, rendered resistance to KAN in H37Rv, an AG-sensitive strain of *Mtb* (7). Here, we report the in vitro characterization of Eis and show that this resistance enzyme has an unprecedented ability to multiacetylate many AGs. We also present structural and mutagenesis studies of Eis, which explain its acetylation mechanism.

Results and Discussion

Unique Multiacetylation of Aminoglycosides by Eis. Eis is a member of a conserved chromosomally encoded family of proteins present in many pathogens (*SI Appendix*, Fig. S2). It is highly divergent from previously characterized AACs. To gain insight into the mechanism of acetylation of AGs by Eis, we first explored its substrate specificity profile by using a wide set of AGs: netilmicin (NET), sisomicin (SIS), neamine (NEA), ribostamycin (RIB), paromomycin (PAR), neomycin B (NEO), KAN, AMK, tobramycin (TOB), hygromycin (HYG), apramycin (APR), spectinomycin (SPT), and streptomycin (STR). Eis efficiently acetylated a broad variety of AGs (all AGs tested, except APR, SPT, and STR; *SI Appendix*, Fig. S1) as observed by spectrophotometric (Fig. 1 and *SI Appendix*, Table S3) and mass spectrometry (*SI Appendix*, Table S2) assays. Remarkably, and to our surprise, Eis catalyzed an unprecedented multiacetylation (di-, tri-, and even tetraacetylation) of its AG substrates. Such multiple acetylation has not been documented for any other known AAC. To confirm the uniqueness of multiacetylation by Eis, we tested six other AACs known to perform monoacetylation at the 2′-, 3-, or 6′ positions (8–16). UV-Visible (UV-Vis) and mass spectrometry assays of these six AACs with the ten AGs that are multiacetylated by Eis, showed only monoacetylation. These reactions were performed under individually optimized conditions with ten equivalents of acetyl-coenzyme A (AcCoA). To assess catalytic specificity of Eis, we measured k_{cat} and K_m values in steady-state kinetic assays monitoring net acetylation of a variety of AGs (*SI Appendix*, Table S3). Catalytic efficiencies (k_{cat}/K_m) varied in a 40-fold range (from 267 M^{-1} s^{-1} for AMK to 10,042 M^{-1} s^{-1} for NET). Most of this variation was due to differences in k_{cat} (a 24-fold range), whereas K_m only displayed a fourfold variation, suggesting that Eis evolved to bind different AGs with similar affinities.

Regiospecificity of Triacetylation of NEA by Eis. To examine the regiospecificity and the potential order of multiacetylation by Eis, we investigated the triacetylation of NEA (Fig. 1). NEA contains four primary amines located at positions 1, 2′, 3, and 6′. The reaction progress was monitored by thin-layer chromatography (TLC) (Fig. 2 and *SI Appendix*, Table S4). By comparing the retention factor (R_f) values of the mono-, di-, and triacetylated NEA species formed over time by Eis to those of 2′-, 3-, and 6′-acetyl-NEA obtained by using monoacetylating enzymes, as well as to 6′,2′-, 6′,3-, and 3,2′-diacetyl-NEA obtained by the sequential use of pairs of these enzymes, we demonstrated that Eis triacetylates NEA, first at the 2′-, then at the 6′-, and, finally, at the 1 position. At a qualitative level, Fig. 2 demonstrates that these acetylations occur at comparable rates.

Because a purified AAC(1) enzyme was not available, and because no triacetylation of NEA was observed by action of AAC(2′)-Ic, AAC(3)-IV, and AAC(6′) in any order, we could

Author contributions: W.C., T.B., O.V.T., and S.G.-T. designed research; W.C., T.B., and V.R.P. performed research; W.C., T.B., O.V.T., and S.G.-T. analyzed data; and T.B., O.V.T., and S.G.-T. wrote the paper.

The authors declare no conflict of interest.

*This Direct Submission article had a prearranged editor.

Data deposition: Coordinates and structure factor amplitudes for the Eis-CoA-acetamide complex have been deposited in the Protein Data Bank, www.pdb.org (PDB ID code 3R1K).

[1]W.C. and T.B. contributed equally to this work.

[2]To whom correspondence may be addressed. E-mail: olegt@umich.edu or sylviegt@umich.edu.

This article contains supporting information online at www.pnas.org/lookup/suppl/doi:10.1073/pnas.1105379108/-/DCSupplemental.

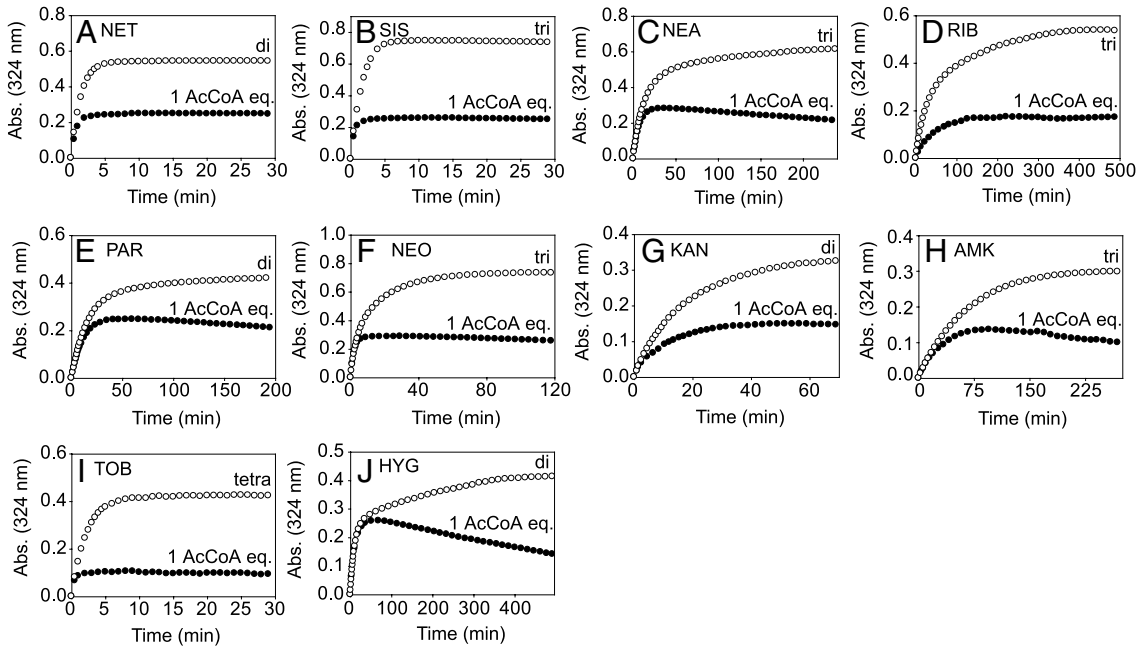

Fig. 1. Multiacetylation of AGs by Eis. Spectrophotometric assay plots monitoring the conversion of various AGs by Eis (black circles) when using one equivalent of AcCoA (*A–J*), and to their di- (*A*, *E*, *G*, and *J*), tri- (*B*, *C*, *D*, *F*, and *H*), and tetraacetylated (*I*) counterparts (white circles) when using 10 equivalents of AcCoA.

not obtain standards of triacetylated NEA. Thus, we scaled-up the enzymatic triacetylation reaction of NEA to unambiguously establish the specific positions on the NEA scaffold acetylated by Eis. The structure was determined from 1-D and 2-D ^{1}H and ^{13}C NMR spectra of the triacetylated NEA purified by flash chromatography. Corresponding spectra of the nonacetylated NEA were used for comparison. This analysis confirmed acetylation of NEA at the 1-, 2′-, and 6′ positions by Eis (*SI Appendix*, Figs. S8–S12 and Tables S5 and S6).

Crystal Structure of Eis. Seeking an understanding of the catalytic mechanism of Eis, we determined a crystal structure of Eis in complex with the reaction products CoA and acetylated HYG, at a resolution of 1.95 Å (Figs. 3 *A–C* and *SI Appendix*, Figs. S13, S14, and Table S7). Eis forms a tightly packed hexamer, in agreement with its hexameric state in solution (*SI Appendix*, Fig. S4). The hexamer resembles a sandwich of two threefold symmetrical trimers (Fig. 3*A*). Overall, 3,800 Å^2 of solvent-accessible surface area of each monomer is buried in the hexameric interface (17), indicating extensive intimate contacts between the monomers. The Eis monomer consists of three regions that are assembled into a heart-shaped molecule (Fig. 3*B*). This shape is formed by an unusual fusion of two general control non-derepressible 5 (GCN5)-related *N*-acetyltransferase (GNAT) regions and a C-terminal region (*SI Appendix*, Fig. S13). The GNAT fold is common among *N*-acetyltransferases in all kingdoms of life. A clearly distinguishable CoA and an acetamide moiety of acetylated HYG in the electron density in the N-terminal GNAT region of Eis are positioned analogously to those found in other AACs (8, 18). This observation indicates that this region is

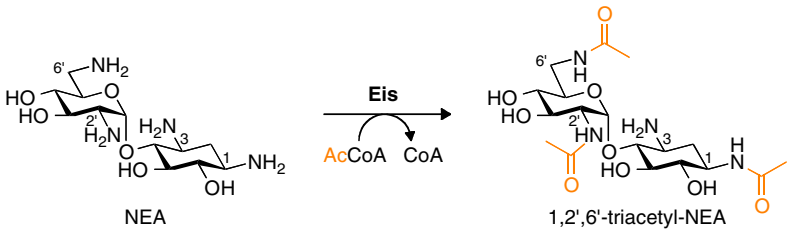

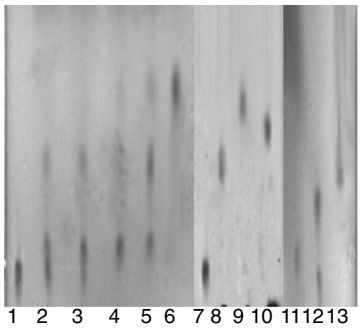

1. NEA (R_f 0.11)
2. NEA + AcCoA + Eis (5 min) (R_f 0.11, 0.14, 0.27)
3. NEA + AcCoA + Eis (10 min) (R_f 0.11, 0.14, 0.27)
4. NEA + AcCoA + Eis (30 min) (R_f 0.14, 0.27)
5. NEA + AcCoA + Eis (2 h) (R_f 0.14, 0.27, 0.39)
6. NEA + AcCoA + Eis (O/N) (R_f 0.39)
7. NEA (R_f 0.11)
8. 6',2'-diacetyl-NEA (R_f 0.27)
9. 6',3-diacetyl-NEA (R_f 0.37)
10. 3,2'-diacetyl-NEA (R_f 0.35)
11. 2'-acetyl-NEA (R_f 0.14)
12. 3-acetyl-NEA (R_f 0.18)
13. 6'-acetyl-NEA (R_f 0.22)

Fig. 2. Conversion of NEA to 1,2′,6′-triacetyl-NEA. TLC time course showing the mono-, di-, and triacetylated NEA products generated by Eis using five equivalents of AcCoA. Control reactions for mono- and diacetylation were performed using AAC(2′)-Ic, AAC(3)-IV, and AAC(6′) individually or sequentially.

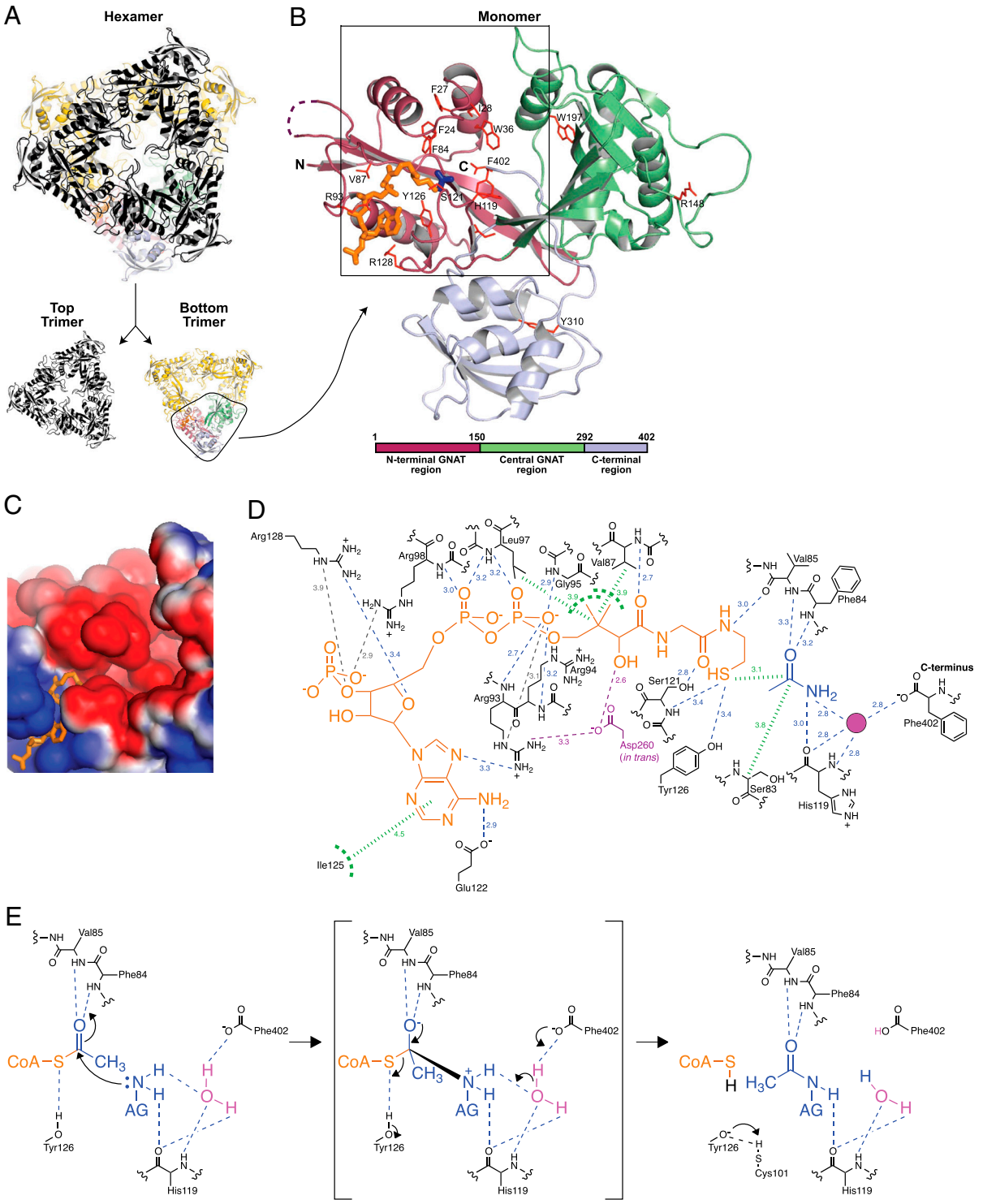

Fig. 3. A crystal structure and a proposed mechanism of Eis. (*A*) A structure of Eis hexamer composed of two trimeric layers as shown in the bottom of this panel. (*B*) The tripartite fold of an Eis monomer bound to CoA (orange sticks) and acetamide (blue sticks). Residues explored in mutagenesis studies are shown as red sticks. (*C*) A zoom-in of the Eis active site (as indicated by the rectangle in *B*). The electrostatic surface of Eis shows the positive charge (blue), negative charge (red), and hydrophobic patches (white). (*D*) Interactions between Eis, CoA, acetamide, and a proposed catalytic water molecule (magenta). Hydrogen bonds, ionic interactions, and hydrophobic contacts are shown by blue, gray, and green dashed lines, respectively. The carboxylate of Asp260 (magenta) from an adjacent monomer in the hexamer makes a hydrogen bond to the Ppant arm of the CoA and forms salt bridges with Arg93 and Arg94 (*in trans*) thereby positioning these Arg residues for binding CoA. (*E*) A proposed mechanism of Eis acetylation.

involved in catalysis. Despite our efforts of crystallization of Eis with many different AGs under a variety of conditions, we did not observe defined electron density for the rest of the AG molecule, reflecting its multiple orientations or flexibility when bound in the active site. The central region of Eis, also resembling a GNAT fold, lacks conserved Arg residues that bind CoA phosphates in this superfamily and, therefore, it is unlikely to be catalytically active. The juxtaposition of the N-terminal and the central GNAT regions creates a large and intricate AG binding pocket (Figs. 3 *B* and *C*). The C-terminal region,

which consists of a 5-stranded β-sheet flanked by four helices on one side, resembles the fold of the animal sterol carrier protein (SCP) (19, 20). However, it lacks the hydrophobic cavity used by SCP to bind lipids. This organization enables the C-terminal peptide of Eis (residues 392–402) to wedge between the two GNAT regions and reach into the active site.

Mechanism of Acetylation by Eis. The bound CoA and the acetamide reveal a network of ionic, hydrophobic, and hydrogen bonding interactions that stabilize the cosubstrate in the Eis active site pocket, and indicate a likely acetylation mechanism (Fig. 3*D*). This mechanism is very similar to that proposed for 2′-*N*-acetylation by AAC(2′)-Ic (8). The AG amino group to be acetylated is ideally positioned by the His119 backbone for a direct nucleophilic attack on the CoA thioester. The tetrahedral transition state is stabilized by polarization of the thioester carbonyl through hydrogen bonding to Phe84 and Val85. As proposed for the *N*-myristoylation mechanism by Nmt1p (21), the C-terminal carboxylate of Phe402 interacts with the amino group through a bridging water molecule and likely serves as a remote base. We propose that the universally conserved Tyr126 at a distance of 3.4 Å from the sulfhydryl group of CoA (3.6 Å in the case of the 2′-*N*-acetylation) likely serves as a general acid to protonate the CoA thiolate.

To probe this mechanism in solution, we first investigated the importance of the proposed catalytic residues Phe402 and Tyr126 (Fig. 4 and *SI Appendix*, Figs. S2, S5, and Table S2). Either the addition of a $CHis_6$ tag or the removal of the three C-terminal amino acid residues (Eis1–399) nearly abolished the acetylation activity of Eis on all AGs tested. These observations confirmed the important role of the C-terminal tail and the Phe402 residue in catalysis. A deletion mutant lacking the C-terminal region (Eis1–311) and the C-terminal region alone (Eis292–402) were also inactive, as expected. The presence of the central GNAT region of Eis indicated a formal possibility that Eis contained a second active site in this region, even though AcCoA coordinating residues were not present. The mutant of the proposed catalytic acid Tyr126Ala completely abolished the acetylation activity on all substrates tested, which agreed with its proposed role in the mechanism and ruled out the possibility of the existence of another active site. We next probed the importance of His119 involved in coordination of the proposed catalytic water molecule (Fig. 3*E*). Mutation of this residue to an Ala resulted in a decrease in activity and a change in the number of acetylated sites (mono- vs. di- vs. tri-) of all AGs tested, thereby confirming its key role in Eis action. Complete inactivity of the Tyr310Ala mutant of the hydrophobic core of Eis indicated that structural stability is crucial for catalytic activity of the enzyme. Similarly, mutating either Trp197 in the hydrophobic core or Asp292 partially buried in the interface of the two GNAT folds to an Ala, almost completely eradicated Eis activity. As another control, we generated an Ala mutant of the surface-exposed Arg148 located far away from any important surface or interface. As expected, we found that this mutation had no significant effect on the Eis activity.

A close examination of the AG binding pocket reveals that it is formed by the adjoining surfaces of the two GNAT folds (Fig. 3*C*). This deep and bifurcated AG binding pocket must allow for AGs of different sizes and structures to be accommodated. The surface of the binding pocket and its entrances are highly negatively charged with occasional hydrophobic patches, which must ensure electrostatic attraction to amine-rich substrates. The residues that line the binding pocket are marked in *SI Appendix*, Fig. S2.

We next inspected the effects of residues lining the AG and AcCoA binding surfaces on the Eis activity by point mutagenesis (Fig. 4 and *SI Appendix*, Fig. S5 and Table S2). Interestingly, although the Phe24Ala mutant drastically decreased acetylation activity, mutations of the neighboring Phe27, Ile28, and Trp36 to Ala did not affect the efficiency of the acetylation reactions, but instead resulted in a change in the number of acetylated sites of many of the AGs tested. These observations are in agreement with the proposed role of these residues in AG binding. In addition, we confirmed that Val87, Arg93, Ser121, and Arg128 all play an important role in AcCoA binding as their mutations to Ala led to a general decrease in catalytic activity of Eis. Finally, the Ala mutation of Phe84 whose backbone amide is proposed to stabilize the oxyanion of the acetyl group of AcCoA and whose side chain is buried in the hydrophobic core, resulted in both a large catalytic deficiency and a change in the number of acetylated sites of most AGs studied.

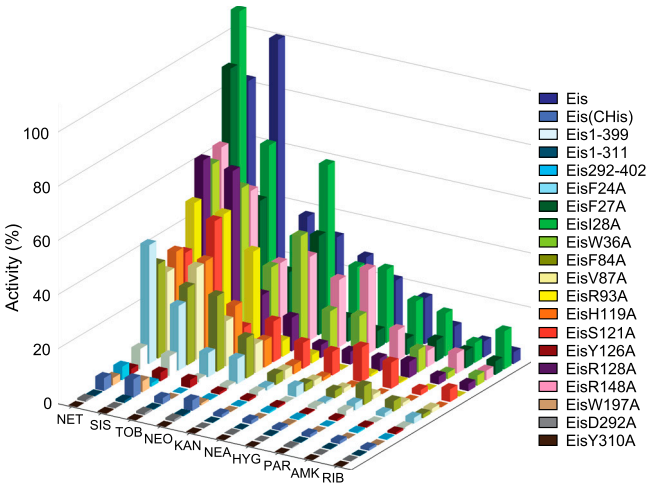

Fig. 4. Relative activity of Eis and its mutants toward the ten tested AGs. All activities are normalized against the acetylation of NET by wild-type Eis.

The biological function of Eis in *Mtb* has been the subject of recent interest (6, 7, 22–29). The biochemical and structural studies described in this report provide clear evidence for an unprecedented multiacetylation capability of Eis that inactivates AG antibiotics. Eis homologues are found in a variety of pathogens that have developed resistance to AGs. Upregulation of *eis* genes in these bacteria may confer resistance to AGs, as observed in *M. tuberculosis*, although such studies have not yet been reported. The unique and efficient strategy of deactivation of AGs by multiacetylation presented herein may be a general, widespread resistance mechanism, and yet another evolutionary hurdle to overcome.

Materials and Methods

Expression and Purification of Eis and Eis Mutants. The *eis* gene (gene locus Rv2416c) was PCR amplified from genomic DNA of *M. tuberculosis* H37Rv and cloned into pET28a. Wild type, Eis mutants, and L-selenomethionine (SeMet)-Eis were overexpressed in BL21(DE3) cells and purified by Ni^{2+} and size-exclusion chromatography. A detailed description of the cloning, mutants generation, Eis expression, and purification can be found in the *SI Appendix*, Figs. S3–S4 and Table S1.

Spectrophotometric Measurements of Acetyltransferase Activity. The acetyltransferase activity of Eis proteins was monitored by a UV-Vis assay in which the free thiol group of CoA, generated by enzyme catalyzed reaction, is coupled to 4,4′-dithiodipyridine to produce thiopyridone monitored by increase in absorbance at 324 nm ($\varepsilon_{324} = 19,800\ M^{-1}\ cm^{-1}$), as described in detail in *SI Appendix*, Fig. S5. The measurements of k_{cat} and K_m values for net acetylation of AGs by Eis were performed by this method, as described in detail in *SI Appendix*, Table S3.

Determination of Number of Sites Acetylated on each AG by Eis Proteins. The number of acetylations was estimated by the above UV-Vis assay and then determined accurately by liquid chromatography mass spectrometry (*SI Appendix*, Table S2). Representative mass spectra are shown in *SI Appendix*, Fig. S6.

Structure Determination of Triacetylated NEA by TLC and NMR. The specific sites for triacetylation of NEA by Eis were directly visualized by comparison with single- and double-acetylated NEA standards (*SI Appendix*, Table S4) produced by regiospecific AACs: AAC(2′)-Ic from *Mtb* (8, 9) (*SI Appendix*, Fig. S7), AAC(3)-IV from *Escherichia coli* (4, 5), AAC(3)-Ib and AAC(6′)-Ib′ from the bifunctional AAC(3)-Ib/AAC(6′)-Ib′ from *Pseudomonas aeruginosa* (12, 13), AAC(6′) from the bifunctional AAC(6′)/AG phosphotransferase (APH)(2″)-Ia from *Staphylococcus aureus* (10, 14), and AAC(6′)-IId from the bifunctional AG nucleotidyltransferase (ANT)(3″)-Ii/AAC(6′)-IId from *Serratia marcescens* (15, 16). A detailed description of the TLC conditions can be found in the *SI Appendix*.

The exact acetyl positions on triacetyl-NEA were confirmed by ^{1}H, ^{13}C, 2-D-total correlation spectroscopy (TOCSY), 2-D-COSY, distortionless enhancement by polarization transfer (DEPT), and heteronuclear correlation (HETCOR) NMR. Proton connectivities were assigned using 2-D-TOCSY and 2-D-COSY spectra. Signals of all carbons were derived from HETCOR and DEPT spectra. The details are given in *SI Appendix*, Figs. S8–S12 and Tables S5–S6.

Crystallization and Structure Determination of the Eis-CoA-Acetamide Complex. Crystals of SeMet-Eis-CoA (grown in the presence of KAN) and Eis-CoA-acetylated HYG (grown with KAN, but subsequently exchanged to HYG in the presence of AcCoA) were grown by the hanging drop method and subsequently flash frozen in liquid nitrogen. Five different AGs were tried in the growth and soaking of the crystals and yielded similar electron density in the Eis active site. The best-diffracting crystals were obtained by using KAN/CoA during growth and HYG/AcCoA during soaking. The crystal structure was determined by the Se single anomalous dispersion method and refined at 1.95 Å resolution for the Eis-CoA-acetylated HYG complex. The details of crystallization and structure determination are described in the *SI Appendix*, Figs. S13–S14 and Table S7.

ACKNOWLEDGMENTS. We thank the staff of sector Life Sciences Collaborative Access Team at the Advanced Photon Source at the Argonne National Laboratory for assistance with the X-ray diffraction data collection. We thank Jacob L. Houghton for help with NMR analysis of 1,2′,6′-triacetyl-NEA. We thank Dr. Tomasz Cierpicki (University of Michigan) for assistance with COSY and TOCSY data collection. This work was supported by the Life Sciences Institute (S.G.-T.) and the College of Pharmacy (S.G.-T. and O.V.T.) at the University of Michigan.

1. Caminero JA, Sotgiu G, Zumla A, Migliori GB (2010) Best drug treatment for multidrug-resistant and extensively drug-resistant tuberculosis. *Lancet Infect Dis* 10:621–629.
2. Houghton JL, Green KD, Chen W, Garneau-Tsodikova S (2010) The future of aminoglycosides: The end or renaissance? *ChemBioChem* 11:880–902.
3. Carter AP, et al. (2000) Functional insights from the structure of the 30S ribosomal subunit and its interactions with antibiotics. *Nature* 407:340–348.
4. Moazed D, Noller HF (1987) Interaction of antibiotics with functional sites in 16S ribosomal RNA. *Nature* 327:389–394.
5. Steitz TA (2008) A structural understanding of the dynamic ribosome machine. *Nat Rev Mol Cell Biol* 9:242–253.
6. Campbell PJ, et al. (2011) Molecular detection of mutations associated with first and second-line drug resistance compared with conventional drug susceptibility testing in *M. tuberculosis*. *Antimicrob Agents Chemother* 55:2032–2041.
7. Zaunbrecher MA, Sikes RD, Jr, Metchock B, Shinnick TM, Posey JE (2009) Overexpression of the chromosomally encoded aminoglycoside acetyltransferase *eis* confers kanamycin resistance in *Mycobacterium tuberculosis*. *Proc Natl Acad Sci USA* 106:20004–20009.
8. Vetting MW, Hegde SS, Javid-Majd F, Blanchard JS, Roderick SL (2002) Aminoglycoside 2′-N-acetyltransferase from *Mycobacterium tuberculosis* in complex with coenzyme A and aminoglycoside substrates. *Nat Struct Biol* 9:653–658.
9. Hegde SS, Javid-Majd F, Blanchard JS (2001) Overexpression and mechanistic analysis of chromosomally encoded aminoglycoside 2′-N-acetyltransferase (AAC(2′)-Ic) from *Mycobacterium tuberculosis*. *J Biol Chem* 276:45876–45881.
10. Green KD, Chen W, Houghton JL, Fridman M, Garneau-Tsodikova S (2010) Exploring the substrate promiscuity of drug-modifying enzymes for the chemoenzymatic generation of N-acylated aminoglycosides. *ChemBioChem* 11:119–126.
11. Magalhaes ML, Blanchard JS (2005) The kinetic mechanism of AAC3-IV aminoglycoside acetyltransferase from *Escherichia coli*. *Biochemistry* 44:16275–16283.
12. Dubois V, et al. (2002) Molecular characterization of a novel class 1 integron containing bla(GES-1) and a fused product of aac3-Ib/aac6′-Ib′ gene cassettes in *Pseudomonas aeruginosa*. *Antimicrob Agents Chemother* 46:638–645.
13. Kim C, Villegas-Estrada A, Hesek D, Mobashery S (2007) Mechanistic characterization of the bifunctional aminoglycoside-modifying enzyme AAC(3)-Ib/AAC(6′)-Ib′ from *Pseudomonas aeruginosa*. *Biochemistry* 46:5270–5282.
14. Boehr DD, Daigle DM, Wright GD (2004) Domain-domain interactions in the aminoglycoside antibiotic resistance enzyme AAC(6′)-APH(2″). *Biochemistry* 43:9846–9855.
15. Centron D, Roy PH (2002) Presence of a group II intron in a multiresistant *Serratia marcescens* strain that harbors three integrons and a novel gene fusion. *Antimicrob Agents Chemother* 46:1402–1409.
16. Kim C, Hesek D, Zajicek J, Vakulenko SB, Mobashery S (2006) Characterization of the bifunctional aminoglycoside-modifying enzyme ANT(3″)-Ii/AAC(6′)-IId from *Serratia marcescens*. *Biochemistry* 45:8368–8377.
17. Tsodikov OV, Record MT, Jr, Sergeev YV (2002) Novel computer program for fast exact calculation of accessible and molecular surface areas and average surface curvature. *J Comput Chem* 23:600–609.
18. Maurice F, et al. (2008) Enzyme structural plasticity and the emergence of broad-spectrum antibiotic resistance. *EMBO Rep* 9:344–349.
19. Choinowski T, Hauser H, Piontek K (2000) Structure of sterol carrier protein 2 at 1.8 Å resolution reveals a hydrophobic tunnel suitable for lipid binding. *Biochemistry* 39:1897–1902.
20. Dyer DH, et al. (2003) The structural determination of an insect sterol carrier protein-2 with a ligand-bound C16 fatty acid at 1.35-A resolution. *J Biol Chem* 278:39085–39091.
21. Bhatnagar RS, Futterer K, Waksman G, Gordon JI (1999) The structure of myristoyl-CoA:protein N-myristoyltransferase. *Biochim Biophys Acta* 1441:162–172.
22. Wei J, et al. (2000) Identification of a *Mycobacterium tuberculosis* gene that enhances mycobacterial survival in macrophages. *J Bacteriol* 182:377–384.
23. Dahl JL, Wei J, Moulder JW, Laal S, Friedman RL (2001) Subcellular localization of the litracellular survival-enhancing Eis protein of *Mycobacterium tuberculosis*. *Infect Immun* 69:4295–4302.
24. Roberts EA, Clark A, McBeth S, Friedman RL (2004) Molecular characterization of the *eis* promoter of *Mycobacterium tuberculosis*. *J Bacteriol* 186:5410–5417.
25. Dahl JL, et al. (2005) The *relA* homolog of *Mycobacterium smegmatis* affects cell appearance, viability, and gene expression. *J Bacteriol* 187:2439–2447.
26. Samuel LP, et al. (2007) Expression, production, and release of the Eis protein by *Mycobacterium tuberculosis* during infection of macrophages and its effect on cytokine secretion. *Microbiology* 153:529–540.
27. Lella RK, Sharma C (2007) Eis (enhanced intracellular survival) protein of *Mycobacterium tuberculosis* disturbs the cross regulation of T-cells. *J Biol Chem* 282:18671–18675.
28. Wu S, et al. (2009) Activation of the *eis* gene in a W-Beijing strain of *Mycobacterium tuberculosis* correlates with increased SigA levels and enhanced intracellular growth. *Microbiology* 155:1272–1281.
29. Shin DM, et al. (2010) *Mycobacterium tuberculosis eis* regulates autophagy, inflammation, and cell death through redox-dependent signaling. *PLoS Pathog* 6:e1001230.